Evaluation of high-velocity plunging jet issuing characteristics as a basis for plunge pool analysis

P. F. A. MANSO[1], E. F. R. BOLLAERT[2], AND A. J. SCHLEISS[3]

ABSTRACT: This paper presents experimental work on the characteristics of jets issuing from water releasing structures. Systematic experimental tests have been performed at near-prototype velocities of up to 30 m/s using a cylindrical jet nozzle. Dynamic pressures were measured along the diameter at the nozzle outlet with an acquisition rate of up to 2 kHz, for different upstream supply conditions. These measurements allowed assessing the mean and fluctuating characteristics of the jet. The influence of supply circuit secondary currents, aeration, and geometrical contraction on jet turbulence intensity and velocity profiles is discussed. The initial turbulence intensity varies from 2 to 8 %, whereas the kinetic energy correction factor ranges from 1.0 to 1.1. Statistical analysis of pressures measurements shows jet core pressures follow fairly well a Gaussian distribution for non-exceedence probabilities between 0.1 and 0.999. The experimental results and an extensive literature survey are used to define issuance parameters relevant for engineering practice.

RESUME: L'article présente travail expérimental sur les caractéristiques de jets issues d'ouvrages d'évacuation d'eau. Essais systématiques ont été réalisés avec un jet cylindrique pour des vitesses quasi-prototype jusqu'à 30 m/s. Des pressions dynamiques ont été mesurées tout au long du diamètre de la buse de sortie avec une fréquence d'échantillonnage jusqu'à 2 kHz pour différentes conditions d'alimentation. Les mesures de pression ont permis d'identifier les caractéristiques moyennes et fluctuantes du jet à l'émission. L'influence des courants secondaires créés par le système d'alimentation, des conditions d'aération et de la contraction imposée à la

[1] Research Associate, Laboratory of Hydraulic Constructions, Ecole Polytechnique Fédérale de Lausanne (EPFL), now at the Instituto Superior Técnico (IST), Technical University of Lisbon, DECivil – SHRHA – CEHIDRO, Av. Rovisco Pais, 1049-001 Lisbon, Portugal, pmanso@civil.ist.utl.pt
[2] Senior Research Associate, Laboratory of Hydraulic Constructions, Ecole Polytechnique Fédérale de Lausanne (EPFL), Switzerland, erik.bollaert@epfl.ch
[3] Full Professor and Director, Laboratory of Hydraulic Constructions, Ecole Polytechnique Fédérale de Lausanne (EPFL), Switzerland, anton.schleiss@epfl.ch

buse, sur l'intensité de turbulence et la distribution de vitesses à la sortie du jet est discutée. L'intensité de turbulence initiale du jet varie de 2 à 8 % et le coefficient de correction de l'énergie cinétique de 1.0 à 1.1. L'analyse statistique des mesures de pression montre que les pressions dans le noyau du jet suivent une distribution gaussienne dans la plage de probabilités de non dépassement de 0.1 à 0.999. Les mesures expérimentales et une revue extensive de littérature ont été utilisées pour la définition de caractéristiques de sortie de jets d'intérêt pour la pratique.

Key-words: dynamic pressures, turbulence intensity, plunging jets, spillways, pressure distribution

Mots-clés: pressions dynamiques, intensité de turbulence, jets plongeants, évacuateurs de crues, distribution de pressions.

1 INTRODUCTION

Appurtenant structures of dams used for flood control and/or reservoir management often make use of plunging jets. The energy of these high-velocity jets is generally dissipated in natural or concrete lined plunge pools. The hydrodynamic loading produced by jet impact on the plunge pool bottom directly influences its design. This loading is governed by jet issuance characteristics, jet deformation in the air and jet diffusion through the downstream water cushion (Hartung and Häusler, 1973). For both natural and man-made plunge pools, it is necessary to ensure that scour or concrete slab damage due to jet impact does not endanger the foundation of the dam and its abutments. Design of plunge pools is traditionally based on physical model testing and assessment of ultimate scour from empirical formulae (Schleiss, 2002). Step-by-step modelling of scour evolution is, however, of increasing importance in practice. To evaluate the spatial and time evolution of scour, as well as the efficiency of counter-measures, key information such as the issuing conditions and the hydrodynamic loading at the water-rock interface for different types of jets, tailwater levels, pool geometries, etc. are required. Recently, Bollaert (2004) and Bollaert and Schleiss (2005) presented a physically based engineering model for evaluation of plunge pool scour as a function of time. This model points out the importance of the characteristics of plunging jets on scour formation. Manso (2006) presented experimental evidence of the reduction of mean and fluctuating pressures transmitted to the rock due to the lateral confinement of jet diffusion in the pool, compared to pools with flat bottom, providing evidence to further develop the mentioned scour model.

The hydrodynamic characteristics of the jet at impact with the downstream water cushion are closely related to jet issuing conditions. The latter define jet deformation in the air (Ervine & Falvey 1987, Zaman 1999, Buratinni et al. 2004), namely jet spreading and jet break-up. Jet behaviour in the air depends mainly on mean jet velocity, air drag and initial jet geometry. These parameters allow estimating the mean trajectory and impact energy, but do not account for the jet deformation required to assess the impact area. Ervine & Falvey (1987) studied the mechanisms of jet spreading and break-up in the air and jet diffusion in the plunge pool. They found that the key parameter governing jet deformation in the air is the jet's initial turbulence intensity, which defines the rate of increase the jet outer limits and the rate of core contraction by respectively outward and inward development of surface disturbances. Turbulence intensity is defined as $Tu = u'/U$ where u' is the root-mean-square (RMS) value of the axial velocity fluctuations and U is the mean axial velocity. It defines the increase rate of jet surface disturbances, hence of its outer limits and core contraction. The degree of break-up is directly related to the jet core size at impact. The extent of the outer limits of the jet defines the zone at impact that is subjected directly to fluctuating pressures. For practice, a compromise is needed between increasing the throw distance (which means keeping the jet as compact as possible) and increasing the wetted impact area (which means enhancing spreading). Rouse et al. (1951) dealt with a similar dilemma for fire monitors and nozzles, by performing systematic experiments. They highlighted the importance of controlling the initial turbulence of the flow. More recently, Zaman (1999) assessed jet spreading from nozzles of various geometries for jet Mach number ranging from 0.3 to 2.0 and concluded .that rectangular jets deform similarly to circular jets for length/width ratios up to 10, except when issuing conditions are significantly changed by inclusion of protrusions at the outlet section.

Issuing conditions also influence jet behaviour after plunging in the water cushion downstream, especially in the case of undeveloped jets at impact with the pool. Jet core diffusion depends on both jet velocity and turbulence at impact (McKeogh and Elsawy 1980, McKeogh and Ervine 1981), which are closely related with the issuing conditions and the travel distance. The higher the turbulence intensity at impact, the faster the diffusion and disintegration of the core. If no core remains at impact with the pool bottom, a fully turbulent two-phase shear layer

impacts the bottom, generating significant pressure fluctuations. In the opposite case, a core remains, generating a high quasi-steady pressure on the bottom, combined with a turbulent shear layer more radially outwards with large pressure fluctuations. The turbulent shear flow in the plunge pool depends on jet turbulence intensity at impact, pool water depth and pool geometry.
Real-life jets and plunge pools may generate hydrodynamic loadings that significantly differ from those obtained from theoretical assumptions based on jet trajectory and 2D jet diffusion in an unbounded medium at rest. Single-point measurements of *Tu* have been obtained by McKeogh & Elsawy (1980), Ervine & Falvey (1987), May & Willoughby (1991) for velocities lower than 10 m/s and Ervine et al. (1997), Bollaert (2002) for velocities up to 30 m/s. They used different instrumentation and velocity ranges, but do not explicitly account for the shape of the velocity profile at emission and eventual interference caused by upstream supply conditions. Recently, Buratinni et al. (2004) studied horizontal air jets with velocities up to 12 m/s and radial *Tu* values of about 2% for unperturbed jets and up to 20% using a large meshed grid. Small mesh grids were reported to reduce jet instability, decrease radial growth and extend the potential core length. Some of their conclusions may be valid for vertical water jets but need experimental validation. To the authors' knowledge, no prototype information on jet *Tu at emission* is available.

The velocity profile at jet issuance is often assumed uniform. Nevertheless, by assuming a fully developed turbulent profile rather than a uniform one, an increase of 10 to 20 % of the maximum impact energy that can be transferred to the rock mass is obtained. The latter assumption is conservative for prototype conditions and substantially increases the jet's erosion potential during the early stages of scour comparing to the former assumption.

This paper provides insight on turbulence intensity and velocity distribution at jet emission by presenting results of extensive systematic experiments with jets at near prototype velocities. Sound insight is obtained on the influence of upstream approach flow conditions, including aeration and outlet geometry. At the end, a summary of jet issuing characteristics for the most encountered hydraulic structures is presented, compiling information from both experimental tests and literature.

2 JET ISSUANCE EXPERIMENTS UNDER NEAR-PROTOTYPE CONDITIONS

2.1 Experimental set-up and test conditions

The objective is to study jet characteristics at issuance from a cylindrical nozzle by means of pressure measurements spatially distributed over the diameter of the nozzle. Prototype jet mean velocities of up to 30 m/s, corresponding to Reynolds numbers of maximum 2E+6 have been used. Pressure measurements were performed at the outlet of a 72 mm diameter jet nozzle using piezo-resistive micro-transducers of type ®KULITE XTL-190-17BAR-A. The transducers have an accuracy of ±0.1 % of the full-scale output (17 bar absolute) due to non-linearity and hysteresis. The transducers' natural resonance frequency is 680 kHz. The acquisition system allowed sampling at a maximum frequency of 20 kHz, the signal being conditioned by a lowpass hardware filter set at the Nyquist frequency. The jet nozzle extends 30 cm out of the supply conduit and 15 cm inside, the ratio between its lengths and diameter is 6.3. The 300 mm diameter conduit upstream supplies a maximum of 120 l/s by means of a 63 m high head pump. Discharge measurements were performed with an electromagnetic flowmeter placed on the supply system, with 1 % accuracy. The measuring pressure transducer was placed in a mobile metallic structure right below the jet supported by a rectangular steel frame (Figure 1). The transducer's tip was aligned vertically with the end section of the outlet nozzle.

The transducer membrane has a measuring diameter of 3.8 mm and is mounted on an elongated 90 mm long hollow stainless steel cylinder. The top of this cylinder is conically shaped to minimize the influence of the cylinder upon the turbulent flow characteristics. Measurements were performed at points evenly spaced of 5 mm, the points closest to the walls were 2 mm from the nozzle inner sidewalls (Table 1). The pressure signal was sampled at 2 kHz during 32.5 sec. Two different supply conditions were tested. The upstream circuit has several 90° bends, which induce secondary currents at the exit for the lowest velocities tested. These conditions have been considered for the first series of tests and were similar to those used by Bollaert (2002). For the second series of tests, a honeycomb grid was placed immediately upstream of the last bend of the supply conduit to reduce the upstream secondary currents by placing. The grid consists of 10 cm long, 10 mm diameter metallic tubes. In addition, an air vent was added at the highest point of the supply system to assure a good and complete ventilation of the conduit, eliminating an eventual source of jet instability.

Table 1 – Test conditions

Test series	Discharge [m^3/s]	Velocity [m/s]	Reynolds [-]	Comments
1st series	0.030	7.37	4.61E+05	13 measurement points spaced by 5 mm
	0.040	9.82	6.15E+05	
	0.050	12.28	7.69E+05	
	0.060	14.74	9.23E+05	
	0.072	17.56	1.10E+06	
	0.081	19.77	1.24E+06	
	0.091	22.35	1.40E+06	
	0.102	24.93	1.56E+06	
	0.114	28.00	1.75E+06	
	0.120	29.47	1.85E+06	
2nd series with an air vent and a honeycomb bundle	0.047	11.62	7.27E+05	15 measurement points by addition of 2 points close to wall
	0.059	14.37	9.00E+05	
	0.071	17.46	1.09E+06	
	0.083	20.48	1.28E+06	
	0.095	23.36	1.46E+06	
	0.107	26.16	1.64E+06	
	0.118	29.08	1.82E+06	
	0.125	30.73	1.92E+06	

On prototype, a large range of jet conditions can be distinguished. For orifices with high Reynolds numbers at emission, the turbulence characteristics of either rectangular or circular jets do not substantially differ, except for hollow jet valves due to their special configuration (Renna et al, 2006). In the case of free overfall weirs, which have relatively low turbulence conditions at issuance, this difference can be more significant. However, since the fall distance is rather long on high-head dams (relatively to the jet break-up length), the jet will often deform towards a circular shape. Circular water jets have been and are object of extensive investigation (McKeogh & Elsawy 1980, Ervine & Falvey 1987, Canepa & Hager 2003, Manso et al. 2004, Bollaert & Schleiss 2003). A quite different situation occurs for jets issuing from ski jumps at the end of long chutes, for which the core is already aerated, reducing surface tension, compactness and enhancing disintegration. The jets produced in the experimental facility show the same behaviour of orifices, free-falling high-velocity undeveloped nappes and submerged outlets encountered in practice, in all cases with non-aerated cores at impact with the pool.

2.2 Mean and fluctuating velocity distributions

Pressure measurements were collected via a multi-channel acquisition card. The signal was conditioned by hardware low-pass filtering at 1 kHz. The filtered signal was digitized by means of an ARCNET PCI 14 bits card.

The jets being rather compact at emission, the pressure transducers measure a highly efficient conversion of kinetic energy head into piezometric head at stagnation. The velocity fluctuations *u'* were obtained from the pressure fluctuations *p'* using Equation 1 proposed by Arndt & Ippen (1970). It neglects higher order terms when converting pressures into velocities with an estimated error of maximum 5 % for a turbulence intensity level of 10 %, which is considered acceptable regarding the expected prototype turbulence intensities.

$$RMS(u') = \sqrt{\overline{u'^2}} = g\,\frac{10\sqrt{\overline{p'^2}}}{U} \qquad (1)$$

In Eq. (1),*p'* is the RMS value of pressure fluctuations [kN/m^2] and g the gravitational acceleration. The mean and RMS pressure values were computed at each measurement position. The time-averaged local velocity V_y at any point along the diameter was derived from Equation 2.

$$V_y = \sqrt{\frac{2(\overline{p} - p_{atm})}{\rho}} \qquad (2)$$

In Eq. (2), ρ is the water density [kg/m^3], $\overline{p}$ the mean local pressure [kN/m^2] and p_{atm} the atmospheric pressure [kN/m^2]. Time-averaged local velocities are estimated within ±0.5 % for *Tu* values of about 10 % (Arndt and Ippen 1970)

The distribution of non-dimensional local outlet velocities is plotted in Figure 2 as a function of *y/D*, in which *D* stands for the nozzle diameter and *y* is the coordinate along the diameter. A comparison is made with data presented by May and Willoughby (1981) for a plane jet. The experimental profiles do not follow theoretical turbulent flow profiles. For velocities lower than 12 m/s, the profiles show very low velocities in the jet core. During the first series of tests, the secondary currents in the supply conduit tend to keep most of the flow close to the outer walls of the nozzle. In the second series of tests, with the honeycomb grid and the air vent, a better flow distribution inside the conduit was achieved for low and intermediate velocities (up to 20 m/s). The grid improves flow homogenisation in the section, rendering the operation of the outlet more regular. The additional head loss did not reduce the range of tested velocities.

For high velocities (V > 25 m/s), the velocity profiles are quasi-uniform, mainly due to the extreme contraction produced by the nozzle. This is more evident from the second series, for which upstream swirling is reduced. Flow is better distributed across the section and a good ventilation of the upstream circuit was assured. No secondary current effects were observed during the second set of tests, most likely due to the combined effect of the grid, the air vent and the contraction.

(Figure 2)

The RMS velocity profiles show a clear reduction of the fluctuating pattern in tests with the grid and air vent. Furthermore, a quite homogeneous repartition of turbulence fluctuations across the section is observed, with some amplification close to the boundaries. Burattini et al. (2004) observed similar amplifications at about 1.5 times the boundary layer thickness from hotwire and anemometer measurements of a jet diameter of 55 mm and a flow velocity of 12.9 m/s. According to Streeter and Wylie (1983), the boundary layer thickness in this case corresponds to $V_y/V_{max} = 0.99$ and is about 4 to 5 mm in the present experimental set-up. Due to the length of the nozzle, the *vena contracta* created downstream of the nozzle entrance may still influence measurements closest to the wall of the nozzle. Measurements at that location exhibit pressure and velocity fluctuations characteristic of flow separation boundaries.

2.3 Pressure distribution

The probability density functions (PDF) of the measured data were computed and compared with the corresponding Gaussian distribution fit, using linear and logarithmic scales, in Figure 3. Placing the grid and adding the air vent seems to slightly increase the (negative modules of the) skewness C_s and further increase the peakedness of the data PDF at $y/D = 0.5$ (jet axis) and $y/D = 0.083$. All presented data series show negative skewness, meaning that asymmetry regarding a standard Gaussian distribution ($\overline{p} = 0$, $RMS\ p' = 1$, $C_s = 0$, $K = 0$) is more pronounced for extreme low pressure values. On the other hand, all but one series present positive relative kurtosis values K, reflecting the peakedness of the functions. The increase in C_s

and in K is the result of enhanced compaction of the jet core (by reduction in swirling and air-water mixture), in agreement with the reduction of RMS values. Jet deflection at the transducer's tip stagnation became more pronounced; in this situation C_s becomes negative, as observed also by Manso et al. (2006a) for impact pressures in pool with flat bottom. Closer to the nozzle boundaries, the PDF functions for low velocities (i.e. V = 10m/s) show relative kurtosis values closer to a Normal fit (K = 0) than at the jet centreline. At the jet axis, the trend is inversed and the PDF functions for high velocities (i.e. V = 30 m/s) show kurtosis closer to the Normal fit at the axis than at the boundaries.

Data PDF at y/D=0.028 without grid and air vent, show the flattest functions (lowest relative kurtosis), namely for low velocities. This is most likely representative of wall turbulence due to interference with the boundary layer or with the *vena contracta* separation zone created by the sudden section contraction.

(Figure 3)

For the highest velocities tested (quasi-prototype high-velocity jets), dynamic pressures at the jet axis seem to fairly agree with the Gaussian distribution, except for extreme probabilities (Figure 4). In fact, for very high non-exceedence probabilities beyond 0.999, pressure values drift from the Gaussian fit. Assuming a Gaussian distribution can lead to an underestimation of necessary extreme pressure values (non-conservative, i.e. lower) for design purposes. For low-pressure extremes such assumption provides also non-conservative (i.e. higher) pressures estimates. Each acquisition run lasted 32.5 sec satisfying ergodicity for the mean value within a 1 % accuracy margin. Nevertheless, it may not be excluded that higher and lower extreme pressure values occur in reality or when larger sampling durations are used.

(Figure 4)

2.4 Turbulence intensity and kinetic energy correction factor

Section-averaged and local turbulence intensities were computed using the mean section-averaged velocity U and the mean local velocity V_y respectively. For section-averaged Tu values, eventual errors depend on both transducer and flowmeter calibration accuracy, whereas for local Tu estimates, only the calibration accuracy of the transducers is concerned. In Figure 5, section-averaged and local turbulence intensities (at the jet axis) are presented. Results of Bollaert (2002) with convergent and pipe nozzles are also included. Jet turbulence intensities are below 8 %, except for velocities lower than 12 m/s. For higher velocities, the results tend to 3 - 4 % for both supply conditions (with/without honeycomb grid). The convergent nozzle reduces turbulence intensities to values of 2 to 3 %.

For comparison, McKeogh & Elsawy (1980) obtained *Tu* values of less than 1 % for laminar jets and 2 % for turbulent jets with velocities lower than 5 m/s, using pressure transducers. May & Willoughby (1991) used a total-head Pitot tube to measure the RMS values of pressure fluctuations and estimated *Tu* in the range of 5.5 to 5.8 % for velocities between 4.9 m/s and 6.6 m/s. Ervine & Falvey (1987) presented initial turbulence intensities of 0.3 % for almost laminar plunging jets, 1.2 % for smooth turbulent plunging jets and 5 % for rough turbulent plunging jets, based on experiments using a laser Doppler velocimeter, velocities from 3.3 m/s up to 29 m/s and a smooth tapered nozzle. The presents results are in good agreement with those of Ervine and Falvey (1987). As an example, their 25 m/s jet had a turbulence intensity estimated at 7 %, which is slightly higher than the present findings with pressure measurements. As prototype velocities and aeration are used, it is assumed that the results are exempt of significant scale effects. It should be kept in mind that local *Tu* estimates depend on the estimate of local velocity V_y which is obtained from an average absolute pressure measurement. These measurements have an inaccuracy margin estimated in 2 % of the transducers' full scale output (i.e. approximately 0.35 bar), including histeresis, non-linearity, zero drift and atmospheric pressure variability (Manso 2006). Therefore, the lower the velocity tested and the mean pressure measured, the larger the relative error of V_y and local *Tu* estimates. RMS statistics are less prone to these sources of inaccuracy, since they represent differences between absolute pressure values taken in relatively short time intervals that may, each one of them, present equal deviations. The differences between *Tu local* values of the present data without grid and air vent and Bollaert (2002)'s observations (i.e. similar conditions) are within the accuracy margin of the pressure measurements. All results present the same trend and converge to *Tu* ~ 3 – 4 % for the range of velocities most relevant for engineering practice.
(Figure 5)

The velocity profiles allow computing the kinetic energy correction factor α.

$$\alpha = \frac{1}{A}\int_A \frac{V_y{}^3}{U^3} dA = \frac{1}{\pi r_0{}^2}\sum_{i=1}^{6}\left(\frac{\frac{V_{i+1}+V_i}{2}}{U}\right)^3 2\pi\left(\frac{r_{i+1}{}^2}{2} - \frac{r_i{}^2}{2}\right) \tag{3}$$

In Equation 3, r_0 is the radius [m] of the nozzle and the velocity profile is assumed valid over the whole cross-section. This coefficient is used to define the kinetic energy and dynamic pressure coefficients of a falling jet impacting in a plunge pool.

For the first series of tests, α is less than 1 for velocities lower than 15 m/s since the flow section is not completely full and core velocities are very low. For velocities higher than 15 m/s, α varies from 1.0 to 1.1 as the influence of the observed secondary currents is reduced. Values close to 1.1 correspond to well-developed turbulent profiles and values close to 1 are typical for uniform profiles (Streeter and Wylie, 1983).

For comparison, Bollaert (2002) found α values of 1.0 at low jet velocities and 1.05 at high jet velocities (up to 30 m/s) with similar supply conditions, performing measurements only under the jet axis and assuming a turbulent velocity profile as given by:

$$\frac{V(y)}{V_{\max}} = \left(\frac{y}{D/2}\right)^{\frac{1}{n}} \tag{4}$$

where $n \approx 7$ (typical value for turbulent rough flows). Streeter and Wylie (1983) presented a value of 1.06 for a 7-power law turbulent velocity profile, whereas May and Willoughby (1991) suggested 1.158 for $n = 6.33$ for plane jets.

Using the honeycomb grid and the air vent, α values are always higher than 1.0 for V > 10 m/s and rapidly decrease to 1.0 for velocities up to 30 m/s.

The turbulence intensity is plotted against the kinetic energy correction factor in Figure 6. These two parameters can be related by means of $Tu = 0.85\ \alpha - 0.824$ for 10 < V < 30 m/s and $Tu = 1.092\ \alpha - 1.071$ for 20 < V < 30 m/s. The first equation was obtained with a correlation factor of $R^2 = 0.947$ and the second with $R^2 = 0.974$ from the results with grid and air vent, both with a confidence interval of 99 %.

(Figure 6)

2.5 Influence of a sudden section contraction and of the upstream supply system

The 17.4 to 1 surface contraction ratio between the supply conduit section and the outlet nozzle section forces the flow to accelerate. According to Chassaing (2000), a contraction accelerates axial flow and reduces the difference between axial fluctuations (either velocity or pressure in compact jets) and lateral (radial) fluctuations while increasing the mean velocity. Turbulence intensity should thus decrease with increasing contraction influence (with the Reynolds number, i.e. with velocity), which is in good agreement with the experimental observations. Since the used contraction is rather sudden than smooth, the velocity profile presents slightly higher velocities close to the sidewalls. The relatively long nozzle length (l/D = 6.25) assures the re-attachement of the streamlines to the nozzle walls upstream from the measuring section, that generally occurs for l/D values larger than 4 - 5 in turbulent pipe flows. Contractions of many different types are often present in large-size hydraulic structures, namely in orifices and other gated structures, and their eventual influence in jet behaviour should be accounted for whenever possible depending on the contraction and nozzle length-to-diameter ratios

Concerning the supply system, the differences between local and average *Tu* values observed at low velocities in the first tests were eliminated by the addition of the honeycomb bundle and the air vent. Power spectral density and time autocorrelation functions were computed for low and high velocities (data series used in figure 3) without and with the honeycomb grid (Manso 2006). Without the grid and air vent, spectra for high velocities shows rather mild slope decrease with frequency of maximum f^{-1}, typical of highly compact jets (Bollaert 2002, Bollaert & Schleiss 2003).The low velocity spectrum is almost flat at intermediate frequencies (up to 80 Hz, log - scales), before sloping down into the dissipation range. This corresponds to an energy transfer from larger to intermediate scales, typical of jet somewhat influenced by geometry-related turbulence. After placing the honeycomb grid, the low and high velocity spectra collapse when divided by the corresponding variances. No isolated energy peaks were observed between 2 and 1000 Hz.

The autocorrelation function at the axis obtained for the first series measurements with V = 10 m/s showed a wavy pattern with a 1 s length, reflecting the unstable behaviour of the jet due to swirling and air entrapment. These oscillations are not present in the autocorrelation function obtained from measurements in similar conditions in the second series of tests.

Interferences of secondary currents, pump regime or oscillations that were present in the first series of tests were eliminated in the second series by addition of the grid and air vent.

3 APPLICATION TO PROTOTYPE JETS

3.1 Introduction

The hydraulic characteristics of seven typical jet-issuing structures are summarized in Table 2. The experimental results were used to compile suggestions for turbulence intensity and kinetic energy correction factor, which may be considered as first-hand indications for design. Designers can use *Tu* to select adequate jet spreading and jet contraction angles for different hydraulic structures in practice, according relationships presented by Ervine et al. (1997) based on the development of jet surface perturbations. Physically–based estimates of the impact area and the degree of jet break up can thus be obtained, which are of utmost importance for plunge pool layout and design. Table 2 is non exhaustive and highlights the absence of sound knowledge on the flow patterns of the most widely used hydraulic structures in large dams. To the authors' knowledge, information on pressure and velocity profiles is qualitative since detailed research is often missing. Particular geometric features (splitters, deflectors, etc.) of each type of outlet are not taken into account and may significantly alter the presented values.

3.2 Overfall weirs

Overfall weirs are characterised by relatively low approach velocities. Flow accelerating over the weir can be considered potential. Along the downstream face, surface roughness initiates boundary layer development. For some cases such as the ogee crest, velocity and pressure at crest level have been systematically studied and assessed. Jets issuing from such structures are often quite compact and non-aerated. For chutes shorter than the distance needed by the turbulent boundary layer to reach the surface (point of inception), the velocity profile in the upper part of the water column corresponds to a non-developed potential flow and is rather uniform (Hager and Vischer 1998). The turbulence intensity is considered very low. The distance from the highest crest point to the inception point measured along the crest and chute may be computed directly as shown by Ferrando and Rico (2002) based on boundary layer thickness development as given by Wood et al. (1983). For a typical case where q = 10 m^2/s, k = 2 mm and θ = 45° a distance of about 54 m would be required to reach inception. In most practical cases of overfall weirs the chute length does not exceed 20 m and the issuing jet may be assumed to have a non-aerated core with a uniform velocity profile and a turbulence intensity of less than 3 % (case 4 in Table 2)

For chutes sufficiently long for the turbulent boundary layer to reach the flow surface, the jet is aerated over depth at issuance and the velocity profile is that of a partially developed turbulent flow (case 5 in Table 2). The turbulence intensity is then about 4-5 % (Ervine and Falvey, 1987).

Non-controlled overtopping of concrete dams may correspond to flow over a broad-crested weir (case 6). Whenever weirs are equipped with jet splitters or deflector blocks issuing conditions are difficult to assess (case 7). These devices reduce the unit discharge and enlarge the streamwise span of the issuing jets, as well as the impact area. They enhance jet disintegration and reduce impacting pressures downstream. Their study by Froude scaled model tests is hardly representative since processes like jet aeration, jet spread and jet break–up largely depend on Weber and Reynolds numbers. The effects of viscosity and surface tension become less relevant only at scales larger than 1/15.

3.3 Orifices

Orifices comprise bottom and intermediate level outlets. Issuing jets are initially non-aerated, save in case of reduced intake submersion. They tend to be operated with full opening of the gates to prevent vibration. Flow streamlines smoothly contract at the intake and the flow accelerates towards the issuance section. The exiting velocity depends on the upstream head. For small gate openings, there is an additional contraction of the streamlines close to the gate. In such case, the velocity profile at issuance is rather uniform and low turbulence intensity values are expected. For large gate openings in orifices of thin arch dams the length of the orifice is around 3 - 6 times its largest dimension (height). In this case, the contraction from the reservoir to the orifice conduit prevails and conditions similar to small gate openings should be found. Jets issuing from high head orifices are considered rough (high Reynolds number), with high mean velocity, rather uniform flow distribution and low turbulence intensity.

For low head orifices (typically less than four times the height of the opening or exiting velocities less than 9 m/s, for which the difference between the velocity at the upper and lower streamlines is larger than 10 %), the contraction will not have such an important role and the flow pattern may exhibit secondary currents. Jets issuing from low head orifices are less affected by streamline contraction and flow acceleration, and are thus more likely to have higher turbulence intensity, eventually with uneven flow distribution due to swirling.

Based of the experimental results, a *Tu* value higher than 8 % should be considered if secondary currents are expected. For low head orifices (case 2), *Tu* should be lower than 8 % if the flow section is fully occupied, values as low as 3 to 4 % being possible for smoothly converging sections producing rough jets. Thus, for high head orifices and bottom outlets (case 3), *Tu* values lower than 4 %, which can reach 2 to 3 % for prototype velocities larger than 30 m/s, can be considered.

3.4 Ski-jumps

The length of the chute being often larger than the distance to the inception point, aeration is either partially or fully developed and quasi-uniform flow conditions may be found at the toe of the chute. For gated structures, Toso and Bowers (1988) estimate the distance needed for the boundary layer to reach the surface to about 50 times the gate opening. At the entrance of the flip bucket, the pressure gradient is hydrostatic and the velocity profile approaches that of a uniform free surface turbulent flow. The mean air concentration is a function of the slope and the characteristics of the water (Falvey 1980). The bucket concave shape deforms the streamlines that tend to remain parallel to the bottom. Streamline contraction deforms the pressure profile from the hydrostatic triangular shape. Some air detrainment may occur. Maximum bottom pressures increase with decreasing invert radii. For equal takeoff angle, most designers rather reduce the radii in the downstream part of bucket to prevent pressure from dropping to inconvenient values (Mason 1993). An extensive study on takeoff angles is presented in Juon and Hager (1998). At issuance, though, one can readily agree that neither the pressure profile is hydrostatic nor the velocity profile is steadily turbulent.

Due to the lack of more sound knowledge, one can assume that these jets have an aerated core with approximately the same mean air content as computed for the chute. The velocity profile may approach the uniform flow shape. Due to the pressure increase, *U* is expected to decrease in the flip-bucket thus increasing *Tu* regarding values at the toe of the chute. The influence of the reduced core density in the trajectory of the issuing jet is a topic of discussion. On one hand, state-of-the-art developments by Ervine et al. (1997) do not apply directly to aerated jet cores and, on the other hand, prototype observations like those done by Kawakami (cited in Martins 1977) are not only few (just two observations) but often lead to an over-conservative correction of the ballistic jet trajectory estimate. For ski jump outlets where no contraction is imposed but the effect of curvature somewhat uniforms the velocity profile, *Tu* values similar to rough jets, i.e. 4 - 8 %, are suggested for feasibility purposes.

4 SUMMARY AND CONCLUSIONS

The complex physics of high-velocity air-water jets demands for prototype scaled studies. Experiments were performed with a circular jet nozzle at prototype velocities of up to 30 m/s to measure dynamic pressures across the jet outlet and to assess hydraulic characteristics of the jet core, such as the velocity profile and the turbulence intensity. The experimental investigations show that:

1) Jet outlet turbulence intensities are generally below 8 %, reaching larger values if the outlet section is either not fully occupied or swirling occurs (secondary flows). For near-prototype velocities, jet turbulence intensities are close to 4 % if the outlet has a pronounced contraction, and close to 2 - 3 % if the outlet is smoothly convergent.
2) An abrupt contraction renders the mean velocity and pressure profiles almost uniform. The kinetic energy correction factor varies between 1.0 and 1.1, which influences the impact kinetic energy downstream. Using a value of 1.1 for design purposes leads to conservative calculations.
3) At very high mean velocities, a more uniform profile corresponds to a lower turbulence intensity.
4) Core pressures follow fairly well a Gaussian distribution for non-exceedence probabilities between 0.1 and 0.999. Extreme pressures drift from a Gaussian distribution. High extreme pressures normally used in design procedures may, still, be fairly estimated with such distribution in the case of compact jets with low turbulence intensity for which the core remains at impact downstream. For most real-life jets, however, this is hardly the case at impact, and extreme pressure distributions should be considered for design.

Based on experimental results and extensive literature survey, a synthesis of hydraulic characteristic for typical structures is presented. Turbulent jet parameters such as initial turbulence intensity and velocity and pressure profiles are described. These allow estimating the jet deformation in the air, the extent of the impact area downstream, the dimensions of the remaining jet core and the resulting jet impact energy downstream. The jets produced in the experimental facility assembled at LCH-EPFL generate near-prototype aeration within the tested range of discharges and jet break-up length. Due to their velocity and turbulence intensity characteristics they entrap as much air in the outer boundary as prototype jets issuing from orifice spillways and free overfall chutes long enough to allow a full development of the boundary layer.

ACKNOWLEDGEMENTS

The experimental work was performed at the LCH-EPFL and co-funded by the grant SFRH/BD/6894/2001 from the *Fundação para a Ciência e a Tecnologia* (FCT, Portugal) and by the *Office fédérale de l'énergie* (OFEN, Switzerland). The fellowship SFRH/BPD/21847/2005 from FCT (Portugal) for the first author as well as the suggestions of Virgilio Fiorotto from the University of Trieste are also acknowledged.

APPENDIX I – REFERENCES

[1] ARNDT, R.E.A. and IPPEN, A.T. (1970). Turbulence measurements in liquids using an improved total pressure probe. *Journal of Hydraulic Research*, 8(2): 131-157.

[2] BOLLAERT, E.F.R. (2002). Transient water pressures in joints and formation of rock scour due to high-velocity jet impact. Ph.D. Thesis No. 2548, *Ecole Polytechnique Fédérale de Lausanne and Communication N° 13 of the Laboratory of Hydr. Constructions (ISSN 1661-1179)*, Lausanne.

[3] BOLLAERT, E. (2004). A comprehensive model to evaluate scour formation in plunge pools." *Hydropower & Dams* (1), 94-101.

[4] BOLLAERT, E. and SCHLEISS, A. (2003). Scour of rock due to the impact of plunging high velocity jets Part II: Experimental results of dynamic pressures at pool bottoms and in one-and two-dimensional closed end rock joints. *Journal of Hydraulic Research*, 41(5), 465-480.

[5] BOLLAERT, E., and SCHLEISS, A. (2005). Physically based model for evaluation of rock scour due to high-velocity jet impact. *Journal of Hydraulic Engineering*, 131(3), 153-165.

[6] BURATTINI, P., ANTONIA, R. A., RAJAGOPALAN, S. and STEPHENS, M. (2004). Effect of initial conditions on the near-field development of a round jet. *Experiments in Fluids* (37), 56-64.

[7] CANEPA, S. and HAGER, W. H. (2003). Effect of air content on plunge pool scour. *Journal of Hydraulic Engineering*, 129(5), 358-365.

[8] CHASSAING, P. (2000). *Turbulence in Fluid Mechanics* (in French), Cépaduès-Editions, Toulouse.

[9] ERVINE, D.A. and FALVEY, H.R. (1987). Behaviour of turbulent water jets in the atmosphere and in plunge pools. *Paper 9136, Water Eng. Group, Proc. of the Institution of Civil Engineers*, Part 2, 83: 295-314.

[10] ERVINE, D. A., FALVEY, H. R., and WITHERS, W. (1997). Pressure fluctuations on plunge pool floors. *Journal Hydraulic Research*, 35(2), 257-279.

[11] FALVEY, H. T. (1980). Air-water flow in hydraulic structures. *Engineering Monograph No. 41*. US Dept. Interior. No. 41: 155 pages.

[12] FERRANDO, A. M., and RICO, J. R. (2002). On the incipient aerated flow in chutes and spillways. *Journal of Hydraulic Research*, 40(1), 95-97.

[13] JUON, R., and HAGER, W. H. (2000). Flip bucket without and with deflectors. *Journal of Hydraulic Engineering*, 126(11), 837-845.

[14] HARTUNG, F. and HÄUSLER, E. (1973). Scours, stilling basins and downstream protection under free overfall jets at dams. *Proc. of the 11th Congress on Large Dams, Madrid, 39-56*.

[15] MANSO, P. A. (2006). The influence of pool geometry and induced flow currents in rock scour by high-velocity plunging jets. Ph.D. Thesis No. 3430, *Ecole Polytechnique Fédérale de Lausanne and Communication N° 25 of the Laboratory of Hydr. Constructions (ISSN 1661-1179)*, Lausanne.

[16] • MANSO, P. A., FIOROTTO, V., BOLLAERT, E.F.R., and SCHLEISS, A. J., (2004), "Effect of jet air content on plunge pool scour", Discussion to S. Canepa and W. H. Hager (2003), *Journal of Hydraulic Engineering*, 130(11): 1128-1130.

[17] MANSO, P. A., BOLLAERT, E. F. R., and SCHLEISS, A. (in print, available online). Impact pressures of high-velocity jets plunging in pools with flat bottom *Experiments in Fluids, doi: 10.1007/s00348-006-0219-5*

[18] MASON, P. J. (1993). Practical guidelines for the design of flip buckets and plunge pools. *Water Power & Dam Construction* (September/October), 40-45.

[19] MAY, R.W.P. and WILLOUGHBY, I.R. (1991). Impact pressures in plunge pool basins due to vertical falling jets. Report SR 242, HR Wallingford, UK.

[20] MCKEOGH, E. J. and ELSAWY, E. M. (1980). Air retained in pool by plunging water jet. *Journal of the Hydraulic Division*. 106 (10): 1577-1593.

[21] MCKEOGH, E. J., and ERVINE, D. A. (1981). Air entrainment rate and diffusion pattern of plunging liquid jets. *Chemical Engineering Science*, 36, 1161-1172.

[22] RENNA, F. M., PIZZUTOLO, O., and MANSO, P.A. (2006) "Dynamic Behaviour of Jets Issued from Howell-Bunger Valves", *Proc. Int. Junior Researcher and Engineer Workshop on Hydraulic Structures (IJREWHS'06),* Montemor-o-Novo, Matos & Chanson (eds.), Report CH61/06, The University of Queensland, Australia: 11-20 (ISBN 1864998687).

[23] ROUSE, H., HOWE, J. W., and METZLER, D. E. (1951). Experimental investigations of fire monitors and nozzles. *Proc. of the ASCE Hydraulic Division*, 77 (Separate 92), 1-29.

[24] SCHLEISS, A. J. (2002). Scour evaluation in pace and time - the challenge of dam designers. *Rock scour due to falling high-velocity jets*, Schleiss & Bollaert, Swets & Zweitinger: 3-22.

[25] STREETER, V. L., and WYLIE, E. B. (1983). *Fluid Mechanics*, Mc-Graw Hill.

[26] TOSO, J. W. and BOWERS, C.E. (1988). Extreme pressures in hydraulic-jump stilling basins. *Journal of Hydraulic Engineering* 114(8): 829-843.

[27] VISCHER, D. L., and HAGER, W. H. (1998). *Dam Hydraulics*, John Wiley and Sons, West Sussex (UK).

[28] WOOD, I. R., ACKERS, P., and LOVELESS, J. (1983). General method for critical point on spillways. *Journal of Hydraulic Engineering*, 109(2), 308-312.

[29] ZAMAN, K. B. M. Q. (1999). Spreading characteristics of compressible jets from nozzles of various geometries. *Journal of Fluid Mechanics*, 383, 197-228.

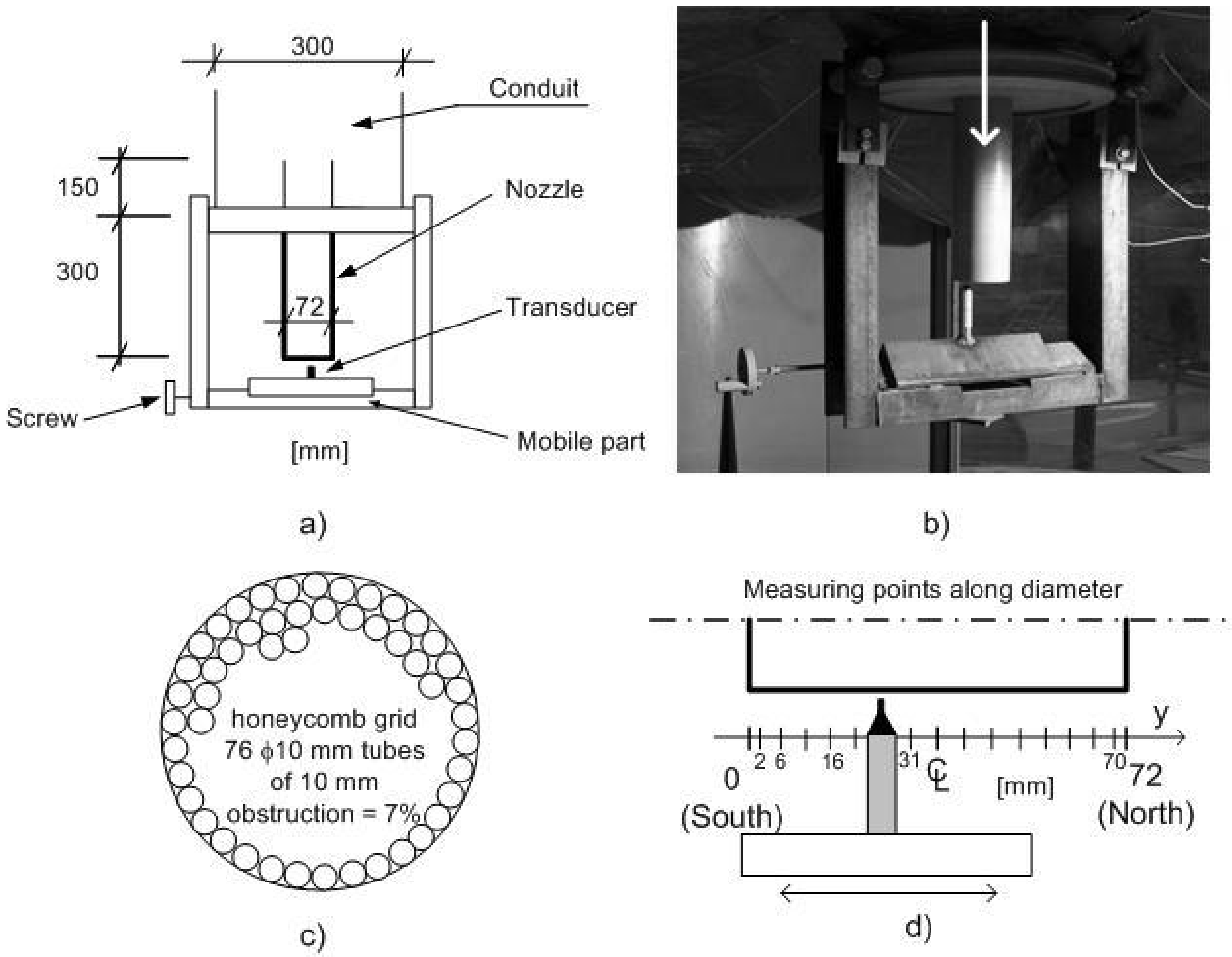

Figure 1. Experimental set-up: a) schematic view and b) photo of the measuring frame under the jet nozzle, c) honeycomb grid which was placed 25 nozzle diameters upstream, d) measuring points spaced of 4 - 5 mm each.

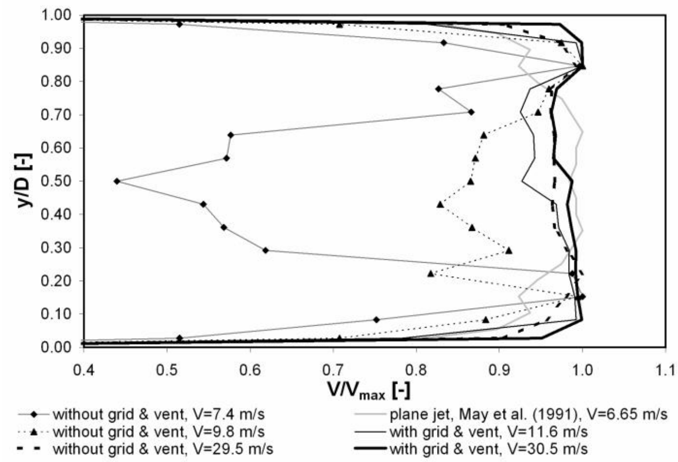

(a)

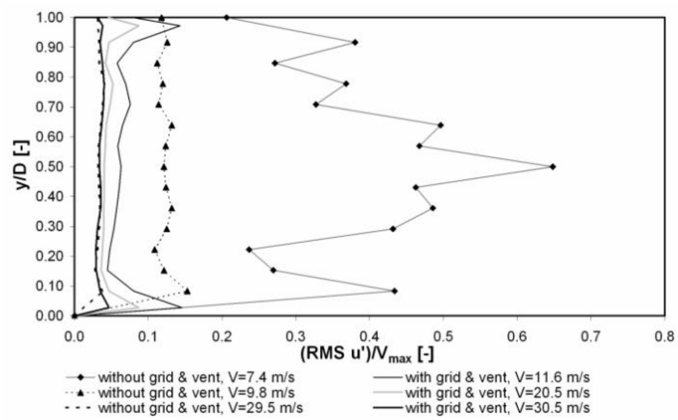

(b)

Figure 2. (a) Mean local velocity obtained from pressure measurements along the diameter (circular jet, 72 mm diameter) compared with data from May & Willoughby (1991, plane jet, 38 mm thickness). (b) RMS velocity profiles. V_{max} is the maximum local velocity in the section.

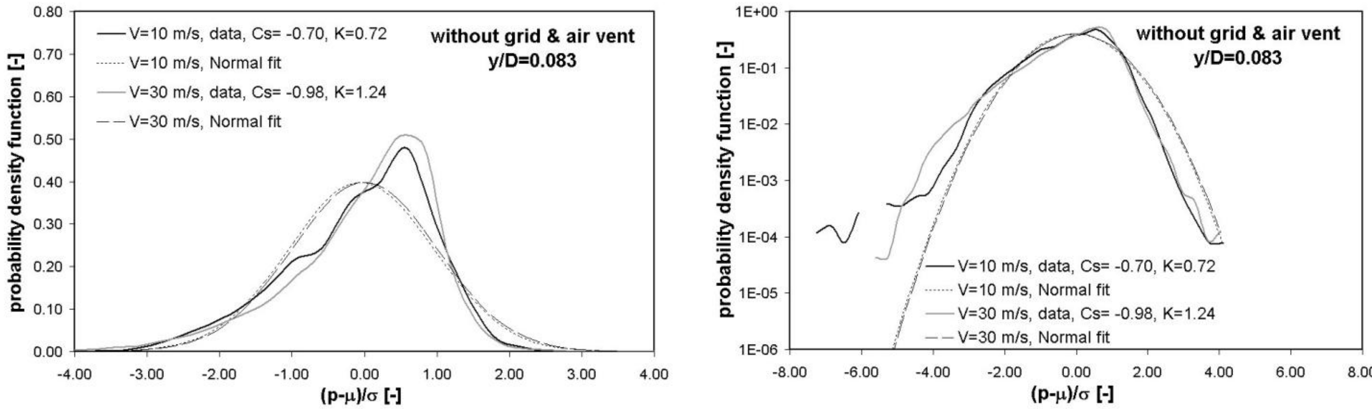
V=10 m/s, data, Cs= -0.70, K=0.72
V=10 m/s, Normal fit
V=30 m/s, data, Cs= -0.98, K=1.24
V=30 m/s, Normal fit
without grid & air vent
y/D=0.083
probability density function [-]
(p-μ)/σ [-]

a)

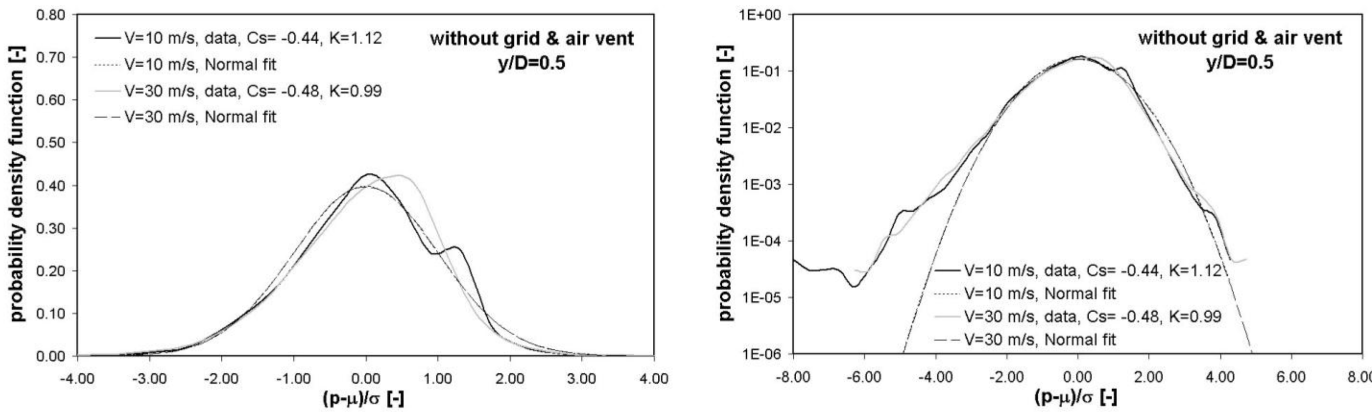
V=10 m/s, data, Cs= -0.44, K=1.12
V=10 m/s, Normal fit
V=30 m/s, data, Cs= -0.48, K=0.99
V=30 m/s, Normal fit
without grid & air vent
y/D=0.5
probability density function [-]
(p-μ)/σ [-]

b)

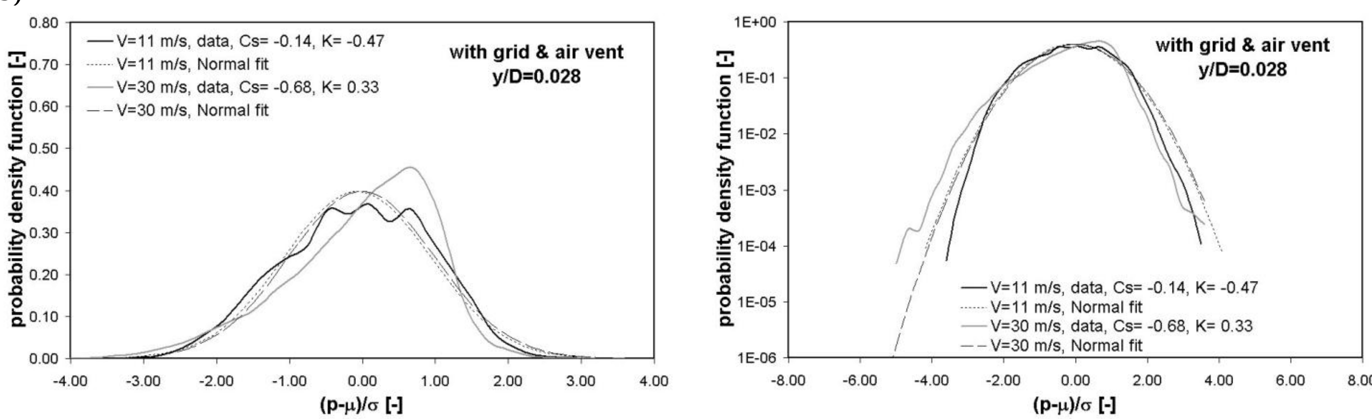
V=11 m/s, data, Cs= -0.14, K= -0.47
V=11 m/s, Normal fit
V=30 m/s, data, Cs= -0.68, K= 0.33
V=30 m/s, Normal fit
with grid & air vent
y/D=0.028
probability density function [-]
(p-μ)/σ [-]

c)

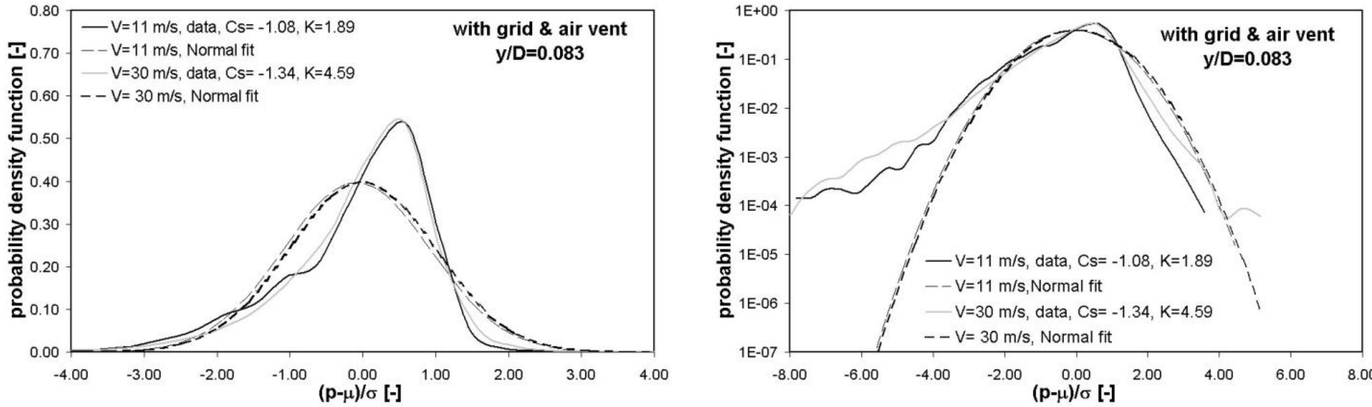

d)

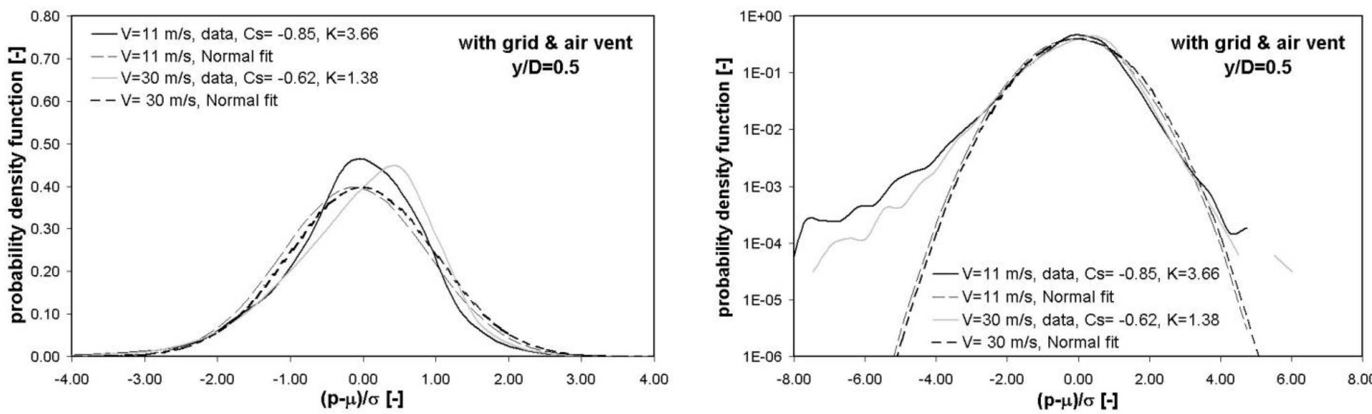

e)

Figure 3: Probability density functions of pressure measurements (using 30 data bins) across the jet compared with the corresponding Normal distribution fits for data series: a) without grid and air vent, y/D=0.083 (6 mm from boundary); b) without grid and air vent, y/D=0.500 (jet axis); c) with grid and air vent, y/D=0.028 (2 mm from boundary); d) with grid and air vent, y/D=0.083 (6 mm from boundary); e) with grid and air vent, y/D=0.500 (jet axis).

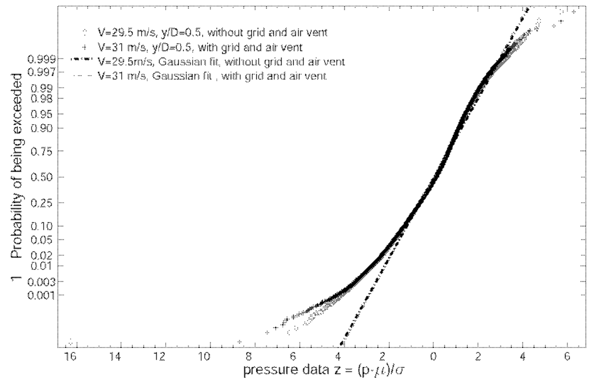

Figure 4: Comparison of pressure data probability at y/D = 0.5 with Gaussian fits, for data series without grid and air vent (V = 29.5 m/s) and with grid and air vent (V = 30.7 m/s).

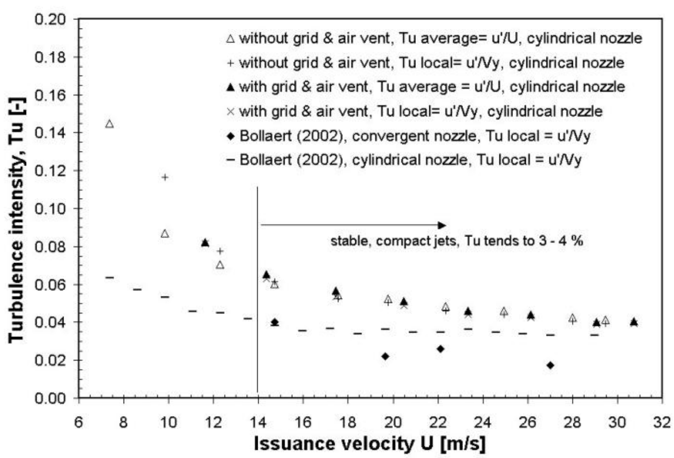

Figure 5. Initial turbulence intensity *Tu* at the jet centreline ($y/D = 0.5$) from pressure measurements as a function of section-averaged mean jet velocity (*Tu* average) and local mean velocity (*Tu* local).

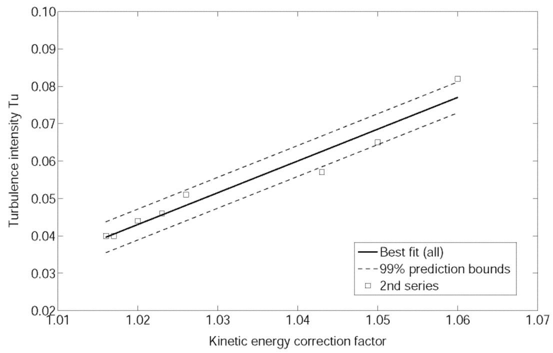

a)

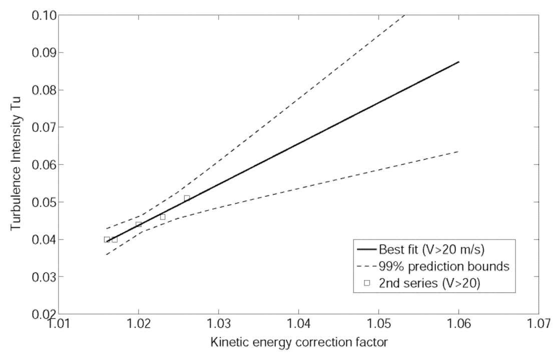

b)

Figure 6. Relationships between section-averaged turbulence intensity Tu and kinetic energy correction factor α for circular jets taking a) Tu values for $10 < V < 30$ m/s and b) $20 < V < 30$ m/s. The velocity profile at issuance is rather uniform (2nd series of measurements). The dashed lines show the prediction bounds for 99 % confidence estimates.

Table 2 – Hydrodynamic characteristics of seven typical spillways and orifices configurations. P(n) and V(n) stand for pressure and velocity profile at issuance, respectively. Initial jet turbulence intensity and kinetic energy correction factor α according to the type of outlet based on experimental results with high-velocity jet flows.

Case	Schematic	Type of jet	Type of Intake	Boundary layer development	Outlet structure	Hydrodynamics	Aeration	Angle of lower nappe	Angle of upper nappe	Turbulence intensity Tu [%]	Kinetic energy correction factor [-]
1			WES weir (gated or non-gated)	Fully or partially developed	Ski jump (plane bucket)	P(n) concave, V(n) deformed logaritmic tending to uniform	Partially or fully aerated core	tang(lip)	approx. tang(lip), eventual correction	4 -8 %, take 4% for high velocities	tending towards 1.0 for high velocities
2	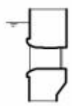	Trajectory	Orifice, low head	Non-developed	Curved lip	P(n) hydrostatic, V(n) turbulent ev. swirling tending to uniform for high V	Depending on submergence	tang(lip)	approx. tang(lip), eventual correction	3 - 8 %	tending towards 1.0 for high velocities
3	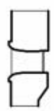		Orifice, high head	Non-developed	Curved lip	P(n) hydrostatic, V(n) quasi uniform	None	tang(lip)	approx. tang(lip), eventual correction	2 – 4 %	approx. 1.0
4			WES weir, short chute	Partially developed	Straight lip	P(n) approx. parabolic, V(n) almost uniform	None	tang(lip)	approx. tang(lip)	Low, < 3 %	approx. 1.0
5		Overfall	WES weir, long chute	Partially or fully developed	Straight or curved lip	P(n) hydrostatic, V(n) turbulent uniform	Partially aerated	tang(lip)	approx. tang(lip)	4 - 5 %	approx. 1.1
6			Broad-crested weir	Non-developed	Straight lip	P(n) approx. parabolic, V(n) freefall quadratic	None	horizontal	approx. 4 to 5°	Low, < 3% but may depend on crest details	approx. 1.0
7		Complex overfall	WES weir	Partially or fully developed	blocks or deflectors	Mixed	Partially or fully aerated	tang(lip)	approx. tang(lip)	8 % overall or more	-

APPENDIX II – NOTATIONS

The following symbols are used in this paper:

A	=	nozzle section surface;
C_s	=	Skewness coefficient
D	=	nozzle diameter;
f	=	Frequency;
g	=	Gravitational acceleration (= 9.8 m/s^2)
K	=	Relative kurtosis coefficient
n	=	from velocity profile Eq. 4;
p	=	total pressure;
$\overline{p}$	=	mean local pressure [kN/m^2];
p'	=	pressure fluctuations;
p_{atm}	=	atmospheric pressure [kN/m^2];
T_u	=	turbulence intensity;
u , U	=	mean flow velocity;
u'	=	velocity fluctuations;
V_y	=	mean local velocity;
V_{max}	=	maximum local velocity across jet section (as in Figure 2);
y	=	radial coordinate of jet section;
α	=	kinetic energy correction factor; and
ρ	=	water density (1000 kg/m^3);